



Article

Future Response of the Wadden Sea Tidal Basins to Relative Sea-Level rise—An Aggregated Modelling Approach

Quirijn J. Lodder^{1,2}, Zheng B. Wang^{1,3,*}, Edwin P.L. Elias³, Ad J.F. van der Spek^{3,4} , Harry de Looff² and Ian H. Townend⁵ 

¹ Faculty of Civil Engineering and Geosciences, Delft University of Technology, 2600 GA Delft, The Netherlands

² Rijkswaterstaat, 3500 GE Utrecht, The Netherlands; quirijn.lodder@rws.nl (Q.J.L.); harry.de.looff@rws.nl (H.d.L.)

³ Deltares, 2600 MH Delft, The Netherlands; edwin.elias@deltares.nl (E.P.L.E.); ad.vanderspek@deltares.nl (A.J.F.v.d.S.)

⁴ Faculty of Geosciences, Utrecht University, 3508 TC Utrecht, The Netherlands

⁵ School of Ocean and Earth Sciences, University of Southampton, Southampton SO14 3ZH, UK; i.townend@soton.ac.uk

* Correspondence: z.b.wang@tudelft.nl

Received: 6 September 2019; Accepted: 17 October 2019; Published: 22 October 2019



Abstract: Climate change, and especially the associated acceleration of sea-level rise, forms a serious threat to the Wadden Sea. The Wadden Sea contains the world's largest coherent intertidal flat area and it is known that these flats can drown when the rate of sea-level rise exceeds a critical limit. As a result, the intertidal flats would then be permanently inundated, seriously affecting the ecological functioning of the system. The determination of this critical limit and the modelling of the transient process of how a tidal basin responds to accelerated sea-level rise is of critical importance. In this contribution we revisit the modelling of the response of the Wadden Sea tidal basins to sea-level rise using a basin scale morphological model (aggregated scale morphological interaction between tidal basin and adjacent coast, ASMITA). Analysis using this aggregated scale model shows that the critical rate of sea-level rise is not merely influenced by the morphological equilibrium and the morphological time scale, but also depends on the grain size distribution of sediment in the tidal inlet system. As sea-level rises, there is a lag in the morphological response, which means that the basin will be deeper than the systems morphological equilibrium. However, so long as the rate of sea-level rise is constant and below a critical limit, this offset becomes constant and a dynamic equilibrium is established. This equilibrium deviation as well as the time needed to achieve the dynamic equilibrium increase non-linearly with increasing rates of sea-level rise. As a result, the response of a tidal basin to relatively fast sea-level rise is similar, no matter if the sea-level rise rate is just below, equal or above the critical limit. A tidal basin will experience a long process of 'drowning' when sea-level rise rate exceeds about 80% of the critical limit. The insights from the present study can be used to improve morphodynamic modelling of tidal basin response to accelerating sea-level rise and are useful for sustainable management of tidal inlet systems.

Keywords: sea-level rise; Wadden Sea; intertidal flat; aggregated modelling

1. Introduction

1.1. Study Area

The Wadden Sea contains the world largest coherent area of tidal flats and spans nearly 500 km along the northern coast of the Netherlands and the North Sea coasts of Germany and Denmark (Figure 1). It is separated from the North Sea by a series of barrier islands, and characterized by a wide variety of channels, sand and mud flats, gullies and salt marshes.

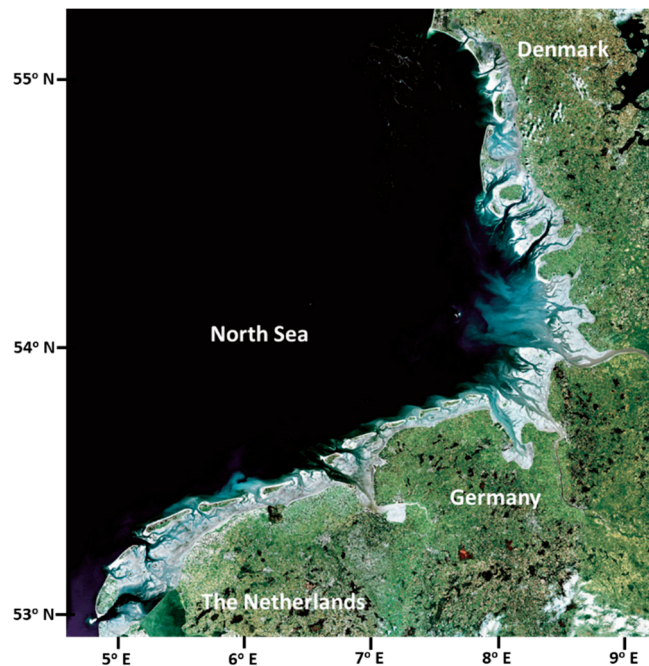


Figure 1. Wadden Sea, the light-colored areas between the barrier islands and the mainland coast (based on picture from www.waddensea-secretariat.org).

The Dutch Wadden Sea, bounded by the tip of the Holland coast in the south and the Ems Estuary in the east, consist of six tidal inlet systems, as indicated in Figure 2. In this sediment-rich system, the inlets all comprise relatively large ebb-tidal delta shoals and narrow and deep inlet channels that are connected to extensive systems of branching channels, tidal flats and salt marshes in the back-barrier basins. Tidal divides (indicated by dotted lines) are formed where the tidal waves travelling through two adjacent inlets meet (Figure 2) and are often considered to form the morphological boundaries of the tidal basins, although model studies (e.g., [1]) and field measurements [2,3] illustrate that net flow is present between the individual basins and may be larger than commonly assumed. The tidal divides are located somewhat eastward of the center of the barrier islands due to the eastward increase of tidal amplitude [4] and the prevailing westerly wind [5].

The tidal flats consist mainly of sand (~90%; grain size 0.10–0.20 mm) and fine-grained muddy sediments (~10%), with decreasing grain size diameters away from the inlet [6–10] due to the settling lag effects of suspended sediments [11–14]. The ebb-tidal deltas primarily consist of sand (0.10–0.40 mm), which is finer on the shoals and coarser in the channels. Similar sand is found in the channels within the basins.

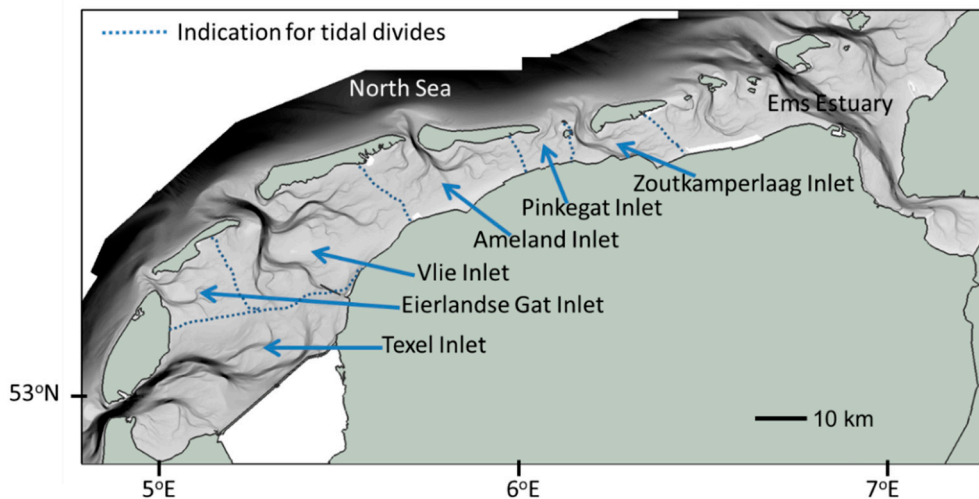


Figure 2. Tidal inlets in the Dutch Wadden Sea (the locations of the tidal divides are indicative).

Following the classification of Davis and Hayes [15], the inlets of the Dutch Wadden Sea belong to the mixed-energy wave-dominated class. Both tides and waves play an important role in shaping and maintaining the Wadden system. The mean tidal range increases from about 1.5 m in the west at the Texel Inlet to 2.2 m in the east at the Zoutkamperlaag. The North Sea wave climate mainly consists of locally generated wind waves with an average significant wave height of about 1.4 m and corresponding peak wave period of about 7 s. The tidal flow is the driving force for the fractal channel patterns in the back-barrier basins [16,17]. For the tidal inlet in morphological equilibrium, the total area of the tidal flats in the basin is related to the basin area; the average height of the tidal flats (measured from low water (LW)) is related to the tidal range; the total volume of channels in the basin and the volume of the ebb-tidal delta are related to the tidal prism [4,18].

1.2. Influence of Sea-Level Rise

Sea-level rise (SLR) has played an important role in the development of the Wadden Sea since its formation more than 7000 years ago [19]. The temperate climate and rising sea level have been essential in the formation of this wetland system. More recently, especially during the last century, human interventions have become important to the formation of the present day Wadden Sea [20,21]. The presence of a wide-variety of (inter) tidal flats, branching channels and salt marshes provide habitats for a wide variety of salt water plants, marine species and birds. Accelerated SLR may threaten this system as the intertidal flats and marshes may become permanently submerged. Observations suggest that some systems remain stable as sediment import and tidal-flat and salt marsh accretion can keep pace with certain rates of relative SLR [19,22–26], while other systems degrade and finally drown [27,28].

Water level measurements over the last 120 years reveal a fairly constant average relative SLR of about 2 mm/y, consisting of about 1.5 mm/y increase of mean sea level and about 0.5 mm/y subsidence [29], along the entire Dutch coast [30–33]. It is anticipated that worldwide SLR will accelerate, although exact rates are still uncertain; a SLR of between 0.3 and 3 m by 2100 has been presented in the literature [34–38]. For the Dutch Wadden Sea, various scenarios, with the SLR rate in 2100 varying from 2 to 20 mm/y, have been presented in [39], highlighting the uncertainties in the future projections of SLR.

Undoubtedly, accelerated SLR will influence the future morphological development of the Wadden Sea. The large intertidal flats in the basins are ecologically important and they help protect against flooding along the mainland coast. Future acceleration of SLR can reduce the intertidal flat area, or even cause the permanent drowning if the rate becomes too high. For the management of the system it is therefore essential to predict the development of the intertidal flats area and the associated

sediment import to the basin for various SLR scenarios, and to evaluate possible mitigating measures for protecting the ecological value of the system and for flood risk management.

Relative SLR in the Wadden Sea is not only caused by global rise of the sea-level and tectonic and isostatic subsidence, but also due to local gas and salt extraction under the Wadden Sea. Extraction permits require that the total relative SLR, i.e., subsidence plus SLR, does not exceed some critical, predefined limit [40], with the aim of ensuring that no significant environmental impact occurs.

It is also anticipated that faster SLR will cause more sediment transport from the North Sea to the Wadden Sea, implying larger sediment losses from the adjacent coasts and barrier islands. Since 1990, the Dutch coastal policy is to maintain the North-Sea coastline at its 1990 position. Erosion of the coastline is counterbalanced with sand nourishments. Acceleration of SLR will thus result in an increase of nourishment volumes. Predicting the increase in these nourishment volumes is essential for future sustainable coastal management.

1.3. Modelling the Response to Sea-Level Rise

Various morphodynamic models have been developed to simulate morphodynamic processes in complex areas such as the Wadden Sea. Generally, three types of models can be distinguished: process-based, aggregated and idealized [21,41–43].

Morphodynamic modelling using process-based models for tidal regions started from the end of the last century [44]. Nowadays, software systems like Delft3D (Deltares, Delft, The Netherlands) [45], are available to simulate morphodynamic changes for rivers, coasts and estuaries. For tidal waters like the Wadden Sea, process-based models have been successful in simulating short-term changes and investigating physical processes and mechanisms for morphological changes [46–49]. Since the pioneering study of Hibma et al. [50] many long-term morphodynamic simulations have been reported in the literature (see e.g., [17,51–58]). However, most of the simulations are carried out for simplified geometry and initial bathymetry, and they mainly concern the morphology at the end of the simulation. Extension of this type of modelling by including SLR (see e.g., [59]) provides qualitative rather than quantitative information about the response of tidal basins to SLR. Predicting the morphodynamics of the Wadden Sea inlets (e.g., Ameland Inlet) over the medium to long-term is still a very challenging task [60,61]. In general, the models are better at predicting the morphodynamic evolution after large-scale disturbances rather than predicting the smaller-scale gradual evolution such as the development of inlets under the influence of SLR. Apparently, process-based morphodynamic models have been set up and calibrated either for reproducing the morphological timescales well (by correctly reproducing the hydrodynamic and sediment transport processes and the short-term morphological changes) or for correctly representing the (characteristics of) morphological equilibrium (end state of the long-term schematized simulations), not both. Models with correct morphological timescales are suitable for simulating evolution after large-scale distortion if their error in representing the morphological equilibrium are much smaller than the distortion. For simulating the response of tidal inlet systems to SLR the model is required to reproduce both the morphological equilibrium as well as the morphological timescale. This implies that most existing process-based morphodynamic (application) models, are in fact, not suitable for simulating responses of tidal inlets to SLR. The only application of process-based models to the Dutch Wadden Sea thus far for simulating impact of SLR [62] predicted an unrealistically low critical rate of SLR because only a single sand fraction was included [63]. Hofstede et al. [64] presented process-based modelling of the impact of future SLR on the (German) Wadden Sea by including sand as well as mud in the model (see also [65]), but their model has not been verified for the response to SLR. Moreover, a general problem with process-based modelling is that due to the complexity of the model and the high computational efforts it is difficult to determine the critical sea-level rise rate for drowning of the tidal flats in the Wadden Sea, even if the model used has been carefully set up and verified.

Idealized models (see review in [66]) are in fact simplified process-based models but they have not been used to model sea-level rise effects on the Wadden Sea, although they are potentially well-suited to the task.

Up to now, the assessment of the impact of relative SLR relies mainly on aggregated morphological models like ASMITA [67–70]. The aggregated scale morphological interaction between tidal basin and adjacent coast (ASMITA) model can be used to determine the critical SLR rate [21,71]. It has also been used to assess the impact of land subsidence quantitatively, as an input to the environmental impact assessment for gas and salt mining projects in the Dutch Wadden Sea [21]. Empirical relations for morphological equilibrium are implemented in this type of model and calibration of the model depends mainly on the morphological timescale, making them better suited for simulating responses to SLR.

The aggregated models also only include one sediment fraction, but they produce more realistic results because their parameter setting is such that the sand-mud mixture is better represented [63]. However, the parameter setting is then, in part, empirically determined during model calibration, rather than being based on observed or theoretically derived values [72]. As pointed out by Wang et al. [72], the validity of the model for certain applications, depends on two characteristics of the field data used for the calibration: the length of the time period covered by the data and the spatial resolution of the data. A major problem is then that the effect of sea-level rise on the morphological development has a very long timescale, at least centuries. Reliable field data over such a long period is not generally available, even for a data-rich system like the Dutch Wadden Sea. Geological data may be used but they can only indicate a range of the critical SLR for a system. Calibrating a morphodynamic model for simulating the effects of sea-level rise using field data of limited duration is therefore still a challenging task.

The study of Van Goor et al. [71] focused on the evaluation of critical SLR rate and did not consider the transient development when the SLR rate changes. In addition, process-based modelling for the effects of SLR is often based on comparison between simulations with different rates of SLR and pays little attention to the transient process when SLR accelerates. However, the transient process can take a long time before a new dynamic equilibrium is established, or the drowning is completed (if the critical SLR rate is exceeded). Knowledge of both the new dynamic equilibrium, and the transient development to the new equilibrium, is important for the management of the system.

The objective of the present study is to improve our insight into the morphological development of the tidal basins in the Dutch Wadden Sea due to accelerated SLR. This will be achieved by analyzing the dynamic morphological equilibrium state and the transient state of a tidal basin when the SLR changes using the ASMITA model. Although, the study focuses on the tidal basins in the Dutch Wadden Sea, the insights obtained are relevant for other similar tidal basins when examined at the aggregated scale implicit in this type of model formulation.

2. Modelling Approach—Aggregated Model ASMITA

The ASMITA (aggregated scale morphological interaction between tidal basin and adjacent coast) model was first proposed by Stive et al. [67] for modelling the long-term morphological development of tidal inlet systems in the Wadden Sea. For a detailed description of the model formulations we refer to [68,69].

ASMITA has a high level of spatial aggregation. A tidal inlet system is schematized into a limited number of morphological elements, similarly to how Walton and Adams [33] describe natural systems. For each element a water volume below a certain reference level or a sediment volume above a certain reference plane acts as a state variable. A tidal inlet is typically schematized into the following three elements (Figure 3):

- The ebb-tidal delta, with its state variable V_d = total excess sediment volume relative to an undisturbed coastal bed profile [L^3];
- The inter-tidal flat area in the tidal basin, with its state variable V_f = total sediment volume between mean low water (MLW) and mean highwater (MHW) [L^3];

- The channel area in the tidal basin, with its state variable $V_c = \text{total water volume below MLW [L}^3\text{]}$.

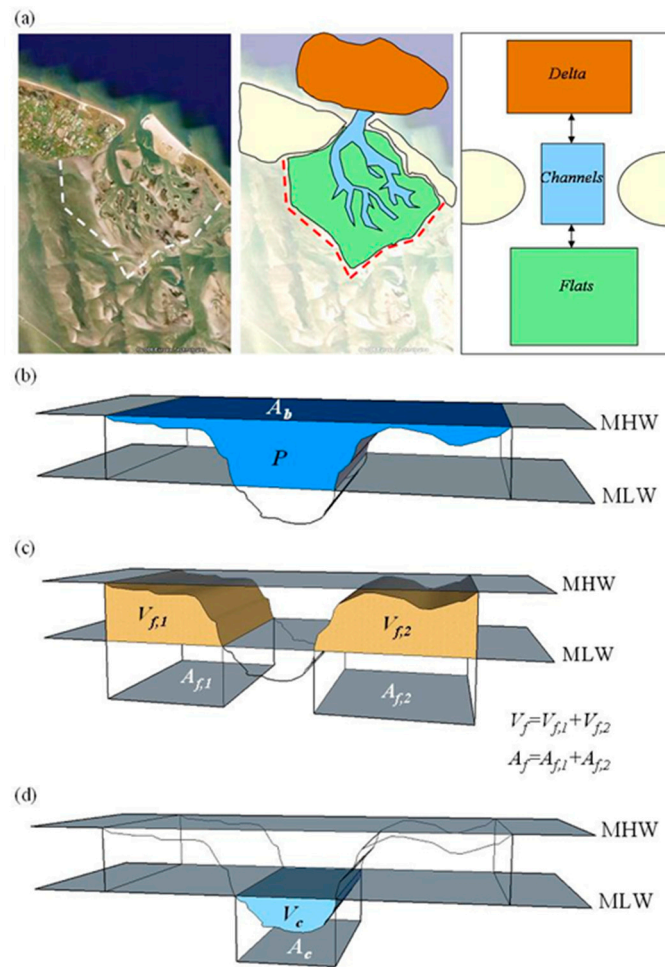


Figure 3. The three-elements schematisation (a) for a tidal inlet in the aggregated scale morphological interaction between tidal basin and adjacent coast (ASMITA) and the definitions of the hydrodynamic and morphological parameters tidal prism P (b), area A_f and volume V_f of tidal flats (c), area A_c and volume V_c of channels (d).

The adjacent coastal areas, which can exchange sediment with the inlet system, are considered as an open boundary, ‘the external world’. For the present analysis the single-element model for the tidal basin with the water volume below highwater V as state variable will be used. Following the definitions (see Figure 3) we have:

$$V = V_c + P \tag{1}$$

As the tidal basins are relatively small compared to the tidal wave length, the tidal prism P can be calculated as:

$$P = 2A_b a - V_f \tag{2}$$

Herein A_b is the basin area and a is the tidal amplitude. As the equilibrium values of V_c and V_f can be calculated from a and P (see [69]), the equilibrium value of V is thus a function of a and A_b :

$$V_e = F(A_b, a) \tag{3}$$

The single element ASMITA model yields (see [58]):

$$\frac{dV}{dt} = \frac{w\delta c_E A_b}{\delta + wA_b} \left[\left(\frac{V_e(t)}{V(t)} \right)^n - 1 \right] + A_b R \tag{4}$$

where

t = time [T];

w = vertical exchange coefficient [LT^{-1}];

δ = horizontal exchange coefficient [L^3T^{-1}];

n = power in the formulation for the local equilibrium concentration [-];

c_E = overall equilibrium concentration [-];

R = relative sea-level rise rate [LT^{-1}].

The power n should be the same as that in a power law relationship between sediment transport rate s and flow velocity u in a process-based model [72]. Its value is an indication of the non-linearity of the relationship. For the general case, in which sediment transport rate is a function of the flow velocity and other factors, such as those indicating the sediment properties, the value of n should be calculated as:

$$n = \frac{\partial s}{\partial u} \frac{u}{s} \quad (5)$$

Many sediment transport formulas may be written as the following general form, with M as a constant coefficient depending on sediment properties and k as a constant.

$$s = M(u - u_c)^k \quad (6)$$

For this relation:

$$n = k \frac{u}{u - u_c} \quad (7)$$

In these relations u_c is the critical flow velocity for incipient movement of sediment particles. It is larger for coarser sediment than for finer sediment. This means that for the same hydrodynamic condition n is larger for coarser sediment than for finer sediment.

3. Analysis and Modelling Results

3.1. Dynamic Equilibrium and Critical SLR Rate

Stive and Wang [68] (see also [21,71]) use Equation (4) to demonstrate that there is a critical limit R_c of sea-level rise rate beyond which the tidal basin will drown:

$$R_c = \frac{w\delta c_E}{\delta + wA_b} \quad (8)$$

Equation (4) can be also be written in terms of depth

$$\frac{dH}{dt} = \frac{w\delta c_E}{\delta + wA_b} \left[\left(\frac{H_e(t)}{H(t)} \right)^n - 1 \right] + R \quad (9)$$

With

$$H = \frac{V}{A_b} \quad \text{and} \quad H_e = \frac{V_e}{A_b} \quad (10)$$

The equations can be made dimensionless using

$$h = \frac{H}{H_e} = \frac{V}{V_e} \quad (11)$$

and

$$\tau = \frac{t}{T} \quad \text{with} \quad T = \frac{V_e}{A_b w c_E} + \frac{V_e}{\delta c_E} = \frac{H_e}{w c_E} + \frac{A_b H_e}{\delta c_E} \quad (12)$$

yielding

$$\frac{dh}{d\tau} = \left[\left(\frac{1}{h} \right)^n - 1 \right] + r \quad (13)$$

herein

$$r = \frac{R}{R_c} \quad (14)$$

It is noted that using Equations (8) and (12) the critical sea-level rise rate can be written as:

$$R_c = \frac{H_e}{T} \quad (15)$$

It should also be noted that the timescale T is not equal to the morphological timescale T_m as defined by linearizing Equation (4) or Equation (9) for the case $R = 0$ [73]. The morphological time scale is the time needed for a small deviation from the morphological equilibrium to decrease by a factor e . The relation between the two timescales is:

$$T = nT_m \quad (16)$$

These relations revealed a number of interesting things worth knowing:

- Equation (15) for R_c revealed the importance of T . In this relation H_e is the equilibrium depth. Empirical relations [69] were available from which its value can be evaluated if the tidal amplitude a and the size of the tidal basin is known, $H_e = F(A_b, a)$. Moreover, it was also connected to direct observations. For basins which are approximately in equilibrium, as, for example, when the basin has not been impacted by human interference for a long time, the equilibrium depth can be evaluated from the measured bathymetry. Note that a correction is necessary when it is in a dynamic equilibrium as it has been forced by sea-level rise with a constant rate for a long time (See Figure 4). An example within the Dutch Wadden Sea is the Ameland Inlet.
- Equation (15) can also be used for estimating the timescale T if R_c can be derived from observations. This is the case for the Texel Inlet, for example, in which a large sediment deficit arose after the closure of the Zuiderzee in 1932 [20,21]. The large sediment deficit (depth of the basin much larger than equilibrium depth, or h much larger than 1) in the basin has practically the same effect on sediment import as a 'drowned' system (see Figure 8), implying that the observed sedimentation rate is close to the critical sea-level rise rate.
- The power n influences the morphological timescale, but not the critical sea-level rise rate. It does influence the dynamic equilibrium state.

In dimensionless form, the dynamic equilibrium morphological state can be derived from Equation (13):

$$h_e = (1 - r)^{-\frac{1}{n}} \quad (17)$$

This relation is shown in Figure 4 which clearly indicates that the dynamic equilibrium morphological state is sensitive to the value of n . If the n value increases, the h_e value for the same dimensionless sea-level rise rate r is smaller. This means that for larger n values, the deviation of the dynamic equilibrium from the morphological equilibrium as defined by the empirical relations is smaller. Figure 4 also shows that for larger n values, the transition from gradual increase to rapid increase of h_e occurred at a larger value of r . However, the magnitude of n also has an influence on the critical SLR rate according to Equations (15) and (16): the larger the n value, the lower the critical rate for the same morphological timescale.

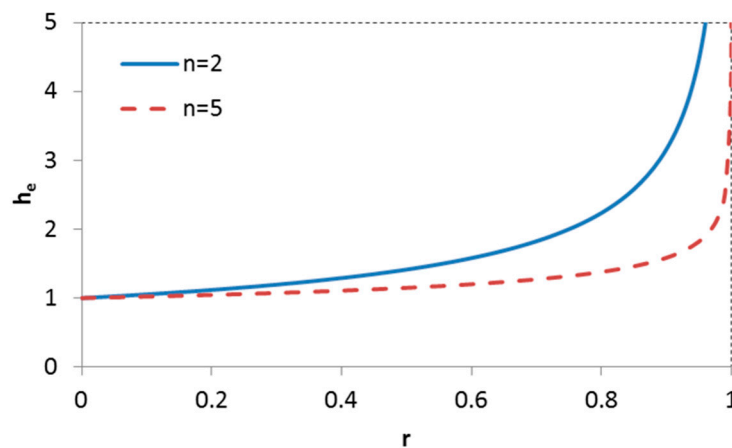


Figure 4. Influence of the power n on the dynamic morphological equilibrium.

3.2. Transient Development

It is also important to know about the time process of the development towards the new dynamic equilibrium when SLR accelerates. Some insight into this process can already be obtained from the morphological timescale, determined by linearizing Equation (13) around $h = h_e$ (the dynamic morphological equilibrium state):

$$\tau_a = \frac{1}{n(1-r)^{\frac{n+1}{n}}} \tag{18}$$

τ_a is the dimensionless time (value of τ) after which a deviation from the dynamic equilibrium would be decreased with a factor e according to the linearized model. For $r = 0$, $\tau_a = 1/n$ which is the same relation between the morphological timescale and the timescale T as given by Equation (16), implying that a larger n results in a smaller morphological timescale, for the same value of T . The morphological timescale depends on the SLR rate r , the larger the r value, the larger the morphological timescale. This means that for a higher accelerated SLR rate it takes longer for the new dynamic morphological equilibrium to be reached.

Figure 5 shows the results of the non-linear model (solution of Equation (13)) for various combinations of n and r . For all the simulations $h(0) = 1$ is used as initial condition, i.e., starting at equilibrium for $r = 0$. The influence of the magnitudes of n and r on the transient development, as indicated by the morphological timescale described above, agrees well with the results of the non-linear model.

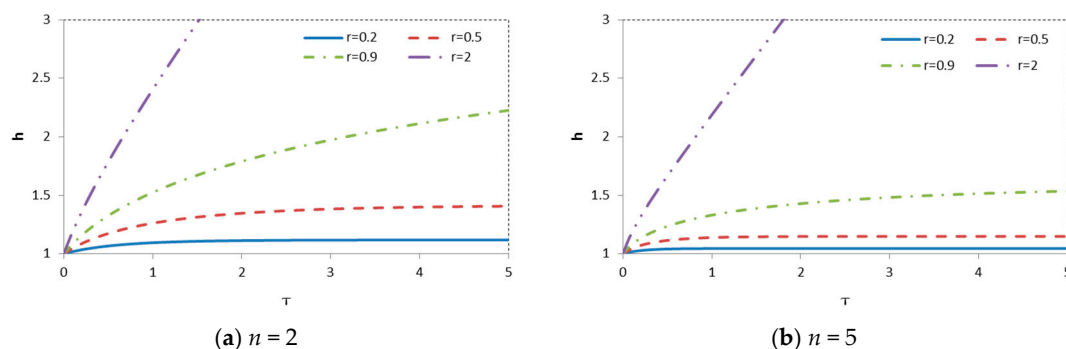


Figure 5. Transient development for various sea-level rise (SLR) rates starting from equilibrium state ($h(0) = 1$). Influence of the power n can be seen by comparing the two panels, (a) for $n = 2$ and (b) for $n = 5$.

Sea-level rise is often considered as a constant value over the past centuries. However, fluctuations are common and it is therefore unlikely that a system is ever completely in equilibrium, especially

if one factors in other forcing conditions (spate river flows, nodal tidal cycles, etc.), even if it is not influenced by human interference. Consequently, it is unlikely that tidal basins are in equilibrium ($h = 1$) at the onset of a period of acceleration, also because of the ongoing SLR. The influence of the initial condition is investigated for four SLR rates (Figure 6), two below and two above the critical rate. For the two cases with SLR rate below the critical rate, a finite dynamic equilibrium depth exists and this state is being achieved in all simulations. However, there are also some notable differences in terms of both the dynamic equilibrium that is reached and the morphological timescale. If SLR is relatively small compared to the critical rate ($r = 0.5$, Figure 6a) the dimensionless timescale is short (about 1.4) and the equilibrium depth is relatively shallow ($h_e = 1.4$). However, if the SLR rate is equal to 90% of the critical value ($r = 0.9$, Figure 6b) then both are larger. The equilibrium depth increases to more than doubled to 3.2, while the dimensionless timescale increases by an order of magnitude to 15.8. When the SLR rate approaches the critical value, the morphological timescale increases to a very large or even infinitely large value (Figure 7).

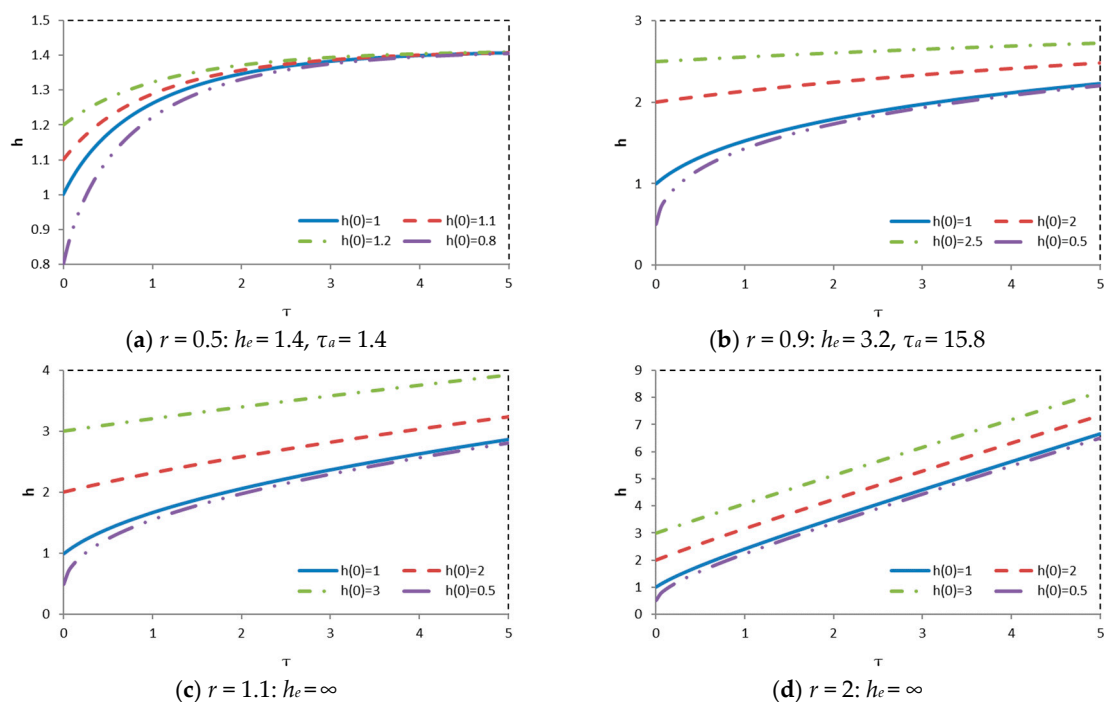


Figure 6. Transient development starting from various initial conditions ($h(0)$) for four SLR rates: (a) $r = 0.5$ (SLR far below critical rate), (b) $r = 0.9$ (SLR just below critical rate), (c) $r = 1.1$ (SLR just above critical rate), (d) $r = 2$ (SLR far above critical rate), in all cases $n = 2$. The dynamic equilibrium h_e and the morphological timescale τ_a are given in the title of the panels.

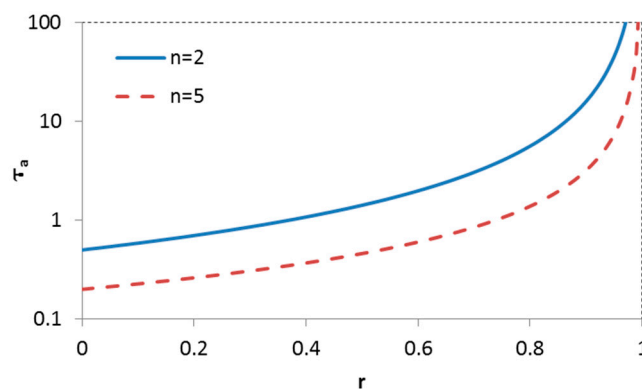


Figure 7. Morphological timescale as function of sea-level rise rate.

For the two cases with SLR greater than the critical SLR rate, no dynamic equilibrium can be reached, and the water depth increases indefinitely. The behavior of the development is not heavily influenced by the initial depth. Especially for the case when the SLR rate is far above the critical rate (Figure 6d) all lines are parallel. In such case, h increases rapidly to a large value and when h is large, the right-hand side of Equation (13) becomes near constant. Physically, this means that there is a maximum rate of sediment transport to the basin, which can be obtained when the water depth in the basin becomes large, implying that further change of the depth has little influence on the sediment transport rate. This can be made clear by considering the two terms on the right-hand side Equation (4). The second term represents the volume increase due to SLR and the first term represents the change due to sediment transport from the basin to the coastal zone. For $V > V_e$, or $h > 1$, it is negative and its magnitude is the sediment import rate to the basin. With the help of Equations (5) and (8) the following relation can be derived for the sediment import rate S (depicted in Figure 8):

$$\frac{S}{S_{\max}} = 1 - \left(\frac{1}{h}\right)^n \quad \text{with } S_{\max} = A_b R_c \text{ is the maximum value of } S \quad (19)$$

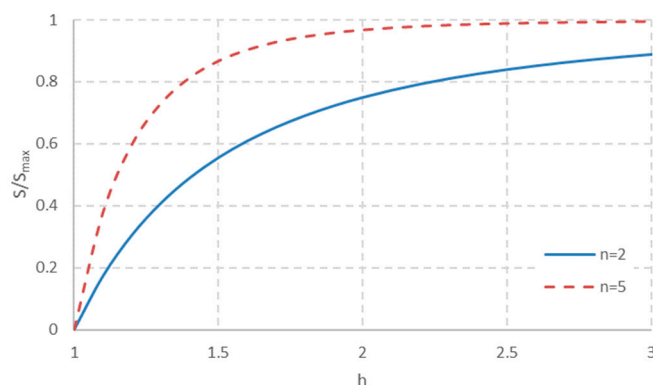


Figure 8. Relation between sediment import rate and the morphological state. $h = 1$ represents the morphological equilibrium without SLR. The import rate approaches the maximum value for large h .

3.3. Application to the Dutch Wadden Sea

It is the dimensionless SLR rate r that influences the behavior of a tidal basin responding to accelerated SLR. This means that the different tidal basins in the Wadden Sea will respond very differently when SLR accelerates, as the SLR rate will be the same but the critical SLR rate for drowning is very different for the different basins. In Table 1, the critical SLR rates for the six tidal basins in the Dutch Wadden Sea (Figure 2), as calculated in [21] are given together with the dimensionless SLR rate r for four SLR rates (2, 4, 6 and 8 mm/y). Figure 9 depicts how the dimensionless SLR rate r increases with the increasing SLR rate R for the various tidal basins in the Dutch Wadden Sea. For the present SLR rate (2 mm/y) r is less than 0.4 for all tidal inlets, so SLR has very limited impact on the Wadden Sea (see Figure 4; Figure 7). For the inlets with large back-barrier basins, Texel Inlet and Vlie, the level above which significant impact of SLR is expected ($r = 0.8$) will be exceeded at a SLR rate R between 4 and 5 mm/y, whereas for the inlets with the smaller basins Pinkegat, Zoutkamperlaag and Eierlandse Gat this level is unlikely to be exceeded.

Table 1. Critical SLR rate for drowning of the various tidal inlet systems in the Dutch Wadden Sea from [21] and the dimensionless SLR rate r for four different SLR rates (2, 4, 6 and 8 mm/y). The equilibrium depth H_e calculated using the empirical relations and the parameters for basin area A_b and tidal range H are also given. The listed time scale T is calculated using the relation with R_c and H_e .

Inlet	A_b (km ²)	H (m)	H_e (m)	R_c (mm/y)	T (Year)	r for SLR Rate =			
						2 mm/y	4 mm/y	6 mm/y	8 mm/y
Texel	655	1.65	2.8	7.00	400	0.29	0.57	0.86	1.14
ELGT	157.7	1.65	1.7	18.0	90	0.11	0.22	0.33	0.44
Vlie	715	1.9	3.5	6.30	560	0.32	0.63	0.95	1.27
Amel	276.3	2.15	2.7	10.4	260	0.19	0.38	0.58	0.77
PinkeG	49.6	2.15	1.7	32.7	55	0.06	0.12	0.18	0.24
ZoutK	105	2.25	2.1	17.1	125	0.12	0.23	0.35	0.47

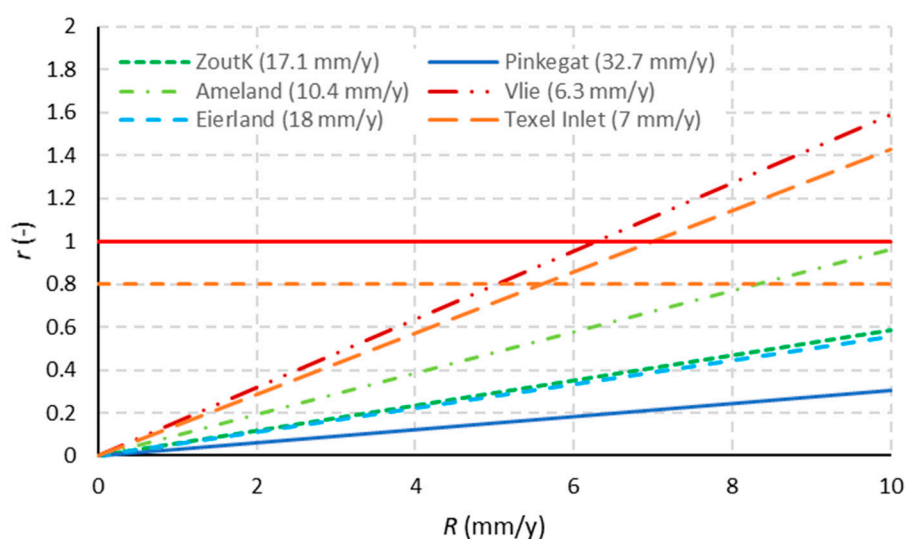


Figure 9. Dimensionless SLR rate r , i.e., normalized with the critical rate (given between brackets in the legend) as calculated in [21] for the tidal inlets in the Dutch Wadden Sea, increases linearly with the SLR rate R . The solid red line ($r = 1$) indicates the initiation of drowning and the dashed orange line ($r = 0.8$) indicates the level above which significant impact of SLR is expected.

Figure 4; Figure 7 suggest that that two indicative limits in the response of tidal basins to SLR can be identified. Below a value of $r = 0.6$ the morphological timescale increases approximately linearly with increasing values of dimensionless SLR rate, r . In contrast, above a value of about $r = 0.8$ the morphological timescale increases rapidly and non-linearly. When r is above this limit, tidal basins will experience a long process of ‘drowning’. In order to ensure that tidal basins remain resilient to accelerating SLR it is advisable to ensure that r does not exceed 0.6 due to anthropogenic causes like gas mining. Wang et al. [21] advised using $r = 0.4$ as the limit for managing gas and salt mining.

4. Concluding Discussions

In summary, the findings from the theoretical analysis provide insights into the response of tidal basins to SLR concerning the critical SLR rate as well as concerning the transient development when SLR rate changes.

The non-linear behavior of the system concerning dynamic morphological equilibrium (Figure 4) and the corresponding morphological timescale (Figure 7) implies that a tidal basin responds to a relatively high SLR rate in a similar way, no matter if the SLR rate is below, equal or above the critical rate (Figure 4). Furthermore, the timescale of the response of tidal basins to changing SLR is very large

(in the order of centuries [73]). It will thus be very difficult if not impossible to determine the critical rate of SLR by monitoring. The present analysis shows that the critical SLR rate can be determined from the morphological equilibrium and the morphological timescale (with respect to morphological equilibrium). The combination of Equations (11) and (12) yields $R_c = H_e/nT_m$. The equilibrium depth H_e can be determined from the field observations, directly or indirectly via empirical relations. The morphological timescale T_m can also be derived from observed development if the considered system is disturbed from its equilibrium. A system can be disturbed not just due to human interventions but also due to, e.g., nodal tidal cycle [74,75], or major storm events [76]. This relation thus makes it possible to determine the critical rate of SLR from field observations of limited time period.

The influence of the power n according to this relation implies that the type of sediment is important. A sandy system can behave very differently to a muddy system. This explains also the findings in [63]: After increasing the n value from two to five the critical SLR rate became much lower even though the model was calibrated to have the same morphological timescale in both cases. This reveals also the importance of sediment grading in tidal systems. Sediment composition varies within tidal basins: fine sediment being found on the flats and coarser fractions in the channels. In order to respond to sea level rise and maintain elevations relative to the tidal frame of reference, the sediment demand of these different zones needs to be met. Hence, a tidal inlet system with a relatively large range in sediment fractions is less vulnerable to drowning than systems with only highly sorted sediment fractions available.

The morphological timescale with respect to the dynamic morphological equilibrium is strongly influenced by the SLR rate. It is essential to realize that it is the morphological timescale with respect to the dynamic morphological equilibrium that determines how long it takes before the new dynamic morphological equilibrium is achieved when SLR accelerates. This morphological timescale is different from the one with respect to the morphological equilibrium for $R = 0$ (i.e., no SLR). It can be estimated by linearizing the model with respect to the dynamic morphological equilibrium. This morphological timescale increases with increasing SLR rate non-linearly (Figure 7). It increases to infinity as SLR rate approaches the critical value. Physically this can be explained by the delayed response of the tidal basin to acceleration of SLR and the limitation of sediment transport capacity through the inlet [21]. The delayed response has the consequence that the effect of acceleration in SLR on sediment exchange between the basin and the coastal area will only be noticeable after a long time. The limit imposed by sediment transport capacity implies that even over the long-term the sediment import to the basin cannot increase in proportion to the SLR rate. For the tidal basin itself it means that acceleration of SLR will cause loss of tidal flat areas, but the total loss will only be achieved after a long period of time. When a basin is drowning, it is importing sediments at the maximum rate and the processes of drowning will be very slow. The availability of sediments to be transported into the basins then becomes important (see the conceptual model in [21]). Tidal basins in this state are perpetually adapting to changing conditions. This helps to explain why tidal basins can exist for centuries to millennia, even with highly changing conditions, as is the case of the Wadden Sea. It is therefore likely that the Wadden Sea tidal basins will persist for a long time even after the process of drowning has started, in the case of strongly accelerated SLR. However, even though a slow drowning process implies no immediate morphological need for mitigation and adaptation, this does not reflect the ecological need and significant changes to the ecosystem may result from these pervasive morphological changes.

It is the dimensionless SLR rate, i.e., the ratio between the SLR rate and the critical rate for drowning, that determines how a tidal basin responds. This means that the morphological responses of the different basins to future accelerated SLR will be very different. For the larger basins Vlie and Texel Inlet, the critical SLR rate is lower and they will likely be seriously affected if SLR rate exceeds 4 mm/y. For the smaller basins, Pinkegat and Eierlandse Gat, the critical SLR rates are high and they are unlikely to be seriously affected by an accelerating SLR. However, the distinguished responses of the different tidal basins to accelerating SLR can only remain if the tidal divides can remain functioning as

boundaries between the neighboring basins. Therefore, it is important to study the more detailed local morphological development around tidal divides.

The insights from the analysis with the aggregated model are also relevant for the process-based modeling. The importance of the correct value of n implies that in a process-based morphodynamic model, it is essential to choose the right sediment transport formulation, and not merely to reproduce the correct order of magnitude of sediment transport rate. Furthermore, it is important that the graded sediment is well represented in the model. The large timescale for achieving the new dynamic equilibrium, especially when the SLR rate is relatively high, makes it impossible to conclude from the model results of limited period if the tidal flats are drowning (total disappearance of tidal flats in the long term) or not. This is confirmed by the findings of Van der Wegen et al. [77] and Elmilady et al. [78] who modelled the development of intertidal flats in San Pablo Bay using a 150 year hindcast and a 100 year forecast, for various SLR scenarios. That (accelerated) SLR rise causes continuous loss of intertidal areas over the forecast period does not necessarily mean that all SLR scenarios are causing drowning of the tidal flats. The simulated period (100 years) can simply be too short compared to the morphological timescale with respect to the dynamic equilibrium.

Author Contributions: Conceptualization, Q.J.L.; data curation, E.P.L.E.; formal analysis, Z.B.W.; funding acquisition, Q.J.L., A.J.E.v.d.S. and Z.B.W.; investigation, Q.J.L.; methodology, Z.B.W. and I.H.T.; project administration, H.d.L.; resources, H.d.L.; validation, Q.J.L. and E.P.L.E.; writing—original draft, Q.J.L. and Z.B.W.; writing—review & editing, all authors.

Funding: This study is carried out within the framework of Coastal Genesis 2 project financed by the Dutch Ministry of Infrastructure and Water Management, and co-founded by NWO via the SEAWAD project (project nr. 14489) and the Dutch Royal Academy of Sciences via the project Coping with Deltas in Transition (project nr. PSA-SA-E-02) within the framework of Programme Scientific Strategic Alliances between China and the Netherlands.

Conflicts of Interest: The authors declare no conflict of interest.

References

1. Duran-Matute, M.; Gerkema, T.; de Boer, G.J.; Nauw, J.J.; Gräwe, U. Residual circulation and freshwater transport in the Dutch Wadden Sea: A numerical modelling study. *Ocean. Sci.* **2014**, *10*, 611–632. [[CrossRef](#)]
2. Van Prooijen, B.C.; Tissier, M.F.S.; de Wit, F.P.; Pearson, S.G.; Brakenhoff, L.B.; Van Maarseveen, M.C.G.; Van der Vegt, M.; Mol, J.W.; Kok, F.; Holzhauer, H.; et al. Measurements of Hydrodynamics, Sediment, Morphology and Benthos on Ameland Ebb-Tidal Delta and Lower Shore face. *Earth Syst. Sci. Data* **2019**. Submitted.
3. Van Weerdenburg, R.J.A. Exploring the relative importance of wind for exchange processes around a tidal inlet system: the case of Ameland Inlet. Msc. Thesis, Delft University of Technology, Delft, The Netherlands, 2019.
4. Wang, Z.B.; Vroom, J.; Van Prooijen, B.C.; Labeur, R.J.; Stive, M.J.F. Movement of tidal watersheds in the Wadden Sea and its consequences on the morphological development. *Int. J. Sediment. Res.* **2013**, *28*, 162–171. [[CrossRef](#)]
5. FitzGerald, D.M. Geomorphic variability and morphologic and sedimentologic controls on tidal inlets. *J. Coast. Res.* **1996**, *23*, 47–71.
6. Van Straaten, L.M.J.U. Sedimentation in tidal flat areas. *J. Alta. Soc. Pet. Geol.* **1961**, *9*, 203–226.
7. De Glopper, R.J. *Over de Bodemgesteldheid Van Het Waddengebied*; Van Zee tot Land 43. Tjeenk Willink: Zwolle, The Netherlands, 1984; 67p.
8. Flemming, B.; Ziegler, K. High-resolution grain size distribution patterns and textural trends in the backbarrier environment of Spiekeroog Island (southern North Sea). *Senckenbergiana Marit.* **1995**, *26*, 1–24.
9. Nyandwi, N. Sediment distribution patterns in the back-barrier areas of the Wadden Sea, Spiekeroog Island, Germany. In *Tidalites: Processes and Products*; Alexander, C., Davis, R.A., Jr., Henry, V.J., Eds.; SEPM (Society for Sedimentary Geology); Special Publication: Tulsa, OK, USA, 1998; Volume 61, pp. 15–22.
10. Bartholomä, A.; Flemming, B.W. Progressive grain-size sorting along an intertidal energy gradient. *Sediment. Geol.* **2007**, *202*, 464–472. [[CrossRef](#)]

11. Postma, H. Transport and accumulation of suspended matter in the Dutch Wadden Sea. *Neth. J. Sea Res.* **1961**, *1*, 148–190. [[CrossRef](#)]
12. Van Straaten, L.M.J.U.; Kuenen, P.H. Accumulation of fine grained sediments in the Dutch Wadden Sea. *Geologie en Mijnbouw* **1957**, *19*, 329–354.
13. Groen, P. On the residual transport of suspended matter by an alternating tidal current. *Neth. J. Sea Res.* **1967**, *3*, 564–574. [[CrossRef](#)]
14. Gatto, V.M.; Van Prooijen, B.C.; Wang, Z.B. Net sediment transport in tidal basins: Quantifying the tidal barotropic mechanisms in a unified framework. *Ocean. Dyn.* **2017**, *67*, 1385–1406. [[CrossRef](#)]
15. Davis, R.A.; Hayes, M.O. What is a wave-dominated coast? *Mar. Geol.* **1984**, *60*, 313–329. [[CrossRef](#)]
16. Cleveringa, J.; Oost, A.P. The fractal geometry of tidal-channel systems in the Dutch Wadden Sea. *Geol. en Mijnb.* **1999**, *78*, 21–30. [[CrossRef](#)]
17. Marciano, R.; Wang, Z.B.; Hibma, A.; De Vriend, H.J. Modeling of channel patterns in short tidal basins. *J. Geophys. Res.* **2005**, *110*, F01001. [[CrossRef](#)]
18. Eysink, W.D. Morphological response of tidal basins to changes. In *Coastal engineering 1990 Procding*; Edge, B.L., Ed.; ASCE: New York, UY, USA, 1990; pp. 1948–1961.
19. Van der Spek, A.J.F.; Beets, D.J. Mid-Holocene evolution of a tidal basin in the western Netherlands: A model for future changes in the northern Netherlands under conditions of accelerated sea-level rise? *Sediment. Geol.* **1992**, *80*, 185–197. [[CrossRef](#)]
20. Elias, E.P.L.; Van der Spek, A.J.F.; Wang, Z.B.; De Ronde, J.G. Morphodynamic development and sediment budget of the Dutch Wadden Sea over the last century. *Neth. J. Geosci.* **2012**, *91*, 293–310. [[CrossRef](#)]
21. Wang, Z.B.; Elias, E.P.L.; Van der Spek, A.J.F.; Lodder, Q.J. Sediment budget and morphological development of the Dutch Wadden Sea-impact of accelerated sea-level rise and subsidence until 2100. *Neth. J. Geosci.* **2018**, *97*, 183–214. [[CrossRef](#)]
22. Nichols, M.M. Sediment accumulation rates and relative sea-level rise in lagoons. *Mar. Geol.* **1989**, *88*, 201–219. [[CrossRef](#)]
23. Canon, D.R.; French, J.R.; Spencer, T.; Reed, D.; Möller, I. Vertical accretion versus elevation adjustment in UK saltmarshes: An evaluation of alternative methodologies. In *Coastal and Estuarine Environments*; Pye, K., Allen, J.R.L., Eds.; Geological Society Special Publications: London, UK, 2000; Volume 175, pp. 223–238.
24. Morris, J.T.; Sundareshwar, P.V.; Nietch, C.T.; Kjerfve, B.; Canon, D.R. Responses of coastal wetlands to rising sea level. *Ecology* **2002**, *83*, 2869–2877. [[CrossRef](#)]
25. Bartholdi, A.T.; Bartholdi, J.; Kroon, A. Salt marsh stability and patterns of sedimentation across a back-barrier platform. *Mar. Geol.* **2010**, *278*, 31–42. [[CrossRef](#)]
26. Madsen, A.T.; Murray, A.S.; Andersen, T.J.; Pejrup, M. Temporal changes of accretion rates on an estuarine salt marsh during the late Holocene—reflection of local sea level changes? The Wadden Sea, Denmark. *Mar. Geol.* **2007**, *242*, 221–233. [[CrossRef](#)]
27. Kentish, M.J. Coastal salt marsh systems in the U.S.: A review of anthropogenic impacts. *J. Coastal Res.* **2001**, *17*, 731–748.
28. Van Wijnen, H.J.; Bakker, J.P. Long-term surface elevation change in salt marshes: A prediction of marsh response to future sea-level rise. *Estuar. Coast. Shelf Sci.* **2001**, *52*, 381–390. [[CrossRef](#)]
29. Baart, F.; Rongen, G.; Hijma, M.; Kooi, H.; de Winter, R.; Nicolai, R. *Zeespiegelmonitor 2018, De Stand Van Zaken Rond de Zeespiegelstijging Langs de Nederlandse Kust*; Deltares en HKV rapport: Delft, The Netherlands, 2019.
30. Deltacommissie, Rapport Deltacommissie. *Dl. 1. Eindverslag en Interimadviezen*; Staatsdrukkerij-en Uitgeverijbedrijf: Hague, The Netherlands, 1960.
31. Deltacommissie. *Working Together with Water, Report of Deltacommissie 2008*; Deltacommissie: Hague, the Netherlands, 2008.
32. Baart, F.; Van Gelder, P.H.; De Ronde, J.; Van Koningsveld, M.; Wouters, B. The effect of the 18.6-year lunar nodal cycle on regional sea-level rise estimates. *J. Coast. Res.* **2012**, *28*, 511–516. [[CrossRef](#)]
33. Walton, T.D.; Adams, W.D. Capacity of inlet outer bars to store sand. In *Proceedings of the Fifteenth Coastal Engineering Conference, Honolulu, HI, USA, 11–17 July 1976*; American Society of Civil Engineers: Reston, VA, USA, 1976; pp. 1919–1936.
34. Meehl, G.A.; Stocker, T.F.; Collins, W.D.; Friedlingstein, P.; Gaye, A.T.; Gregory, J.M.; Kitoh, A.; Knutti, R.; Murphy, J.M.; Noda, A.; et al. Global climate projections. In *Climate Change 2007, the Physical Science Basis. Contribution of Working Group I to the Fourth Assessment Report of the Intergovernmental Panel on Climate Change*;

- Solomon, S., Qin, D., Manning, M., Chen, Z., Marquis, M., Averyt, K.B., Tignor, M., Miller, H.L., Eds.; Cambridge University Press: Cambridge, UK, 2007; pp. 747–845.
35. Church, J.A.; Clark, P.U.; Cazenave, A.; Gregory, J.M.; Jevrejeva, S.; Levermann, A.; Merrifield, M.A.; Milne, G.A.; Nerem, R.S. Sea level change. In *Climate Change 2013, the Physical Science Basis. Contribution of Working Group I to the Fifth Assessment Report of the Intergovernmental Panel on Climate Change*; Stocker, T.F., Qin, D., Plattner, G.-K., Tignor, M., Allen, S.K., Boschung, J., Nauels, A., Xia, Y., Bex, V., Midgley, P.M., Eds.; Cambridge University Press: Cambridge, UK, 2013; pp. 1137–1216.
 36. KNMI. Extreme Zeespiegelstijging in de 21e Eeuw. Koninklijk Nederlands Meteorologisch Instituut (KNMI). News Item, 6 April 2017. Available online: <http://knmi.nl/over-het-knmi/nieuws/extreme-zeespiegelstijging-in-de-21e-eeuw> (accessed on 20 July 2019).
 37. Le Bars, D.; Drijfhout, S.; De Vries, H. A high-end sea level rise probabilistic projection including rapid Antarctic ice sheet mass loss. *Environ. Res. Lett.* **2017**, *12*, 044013. [[CrossRef](#)]
 38. IPCC. Summary for Policymakers. In *IPCC Special Report on the Ocean and Cryosphere in a Changing Climate*; Pörtner, H.-O., Roberts, D.C., Masson-Delmotte, V., Zhai, P., Tignor, M., Poloczanska, E., Mintenbeck, K., Nicolai, M., Okem, A., Petzold, J., et al., Eds.; IPCC: Geneva, Switzerland, 2019; In Press.
 39. Vermeersen, L.L.A.; Slangen, A.B.A.; Gerkema, T.; Baart, F.; Cohen, K.M.; Dangendorf, S.; Duran-Matute, M.; Frederikse, T.; Grinsted, A.; Hijma, M.P.; et al. Sea level change in the Dutch Wadden Sea. *Neth. J. Geosci.* **2018**, *97*, 79–127. [[CrossRef](#)]
 40. De Waal, J.A.; Roest, J.P.A.; Fokker, P.A.; Kroon, I.C.; Muntendam-Bos, A.G.; Oost, A.P.; Van Wirdum, G. The effective subsidence capacity concept: How to assure that subsidence in the Wadden Sea remains within defined limits? *Neth. J. Geosci./Geol. en Mijnb.* **2012**, *91*, 385–399. [[CrossRef](#)]
 41. De Vriend, H.J. Mathematical modeling of meso-tidal barrier islands coasts. Part 1: Empirical and semi-empirical models. In *Advances in Coastal and Ocean Engineering*; Liu, P.L.F., Ed.; World Scientific Publishing Company: Singapore, 1996; pp. 115–149.
 42. De Vriend, H.J.; Ribberink, J.S. Mathematical modeling of meso-tidal barrier island coasts. Part II: Process-based simulation models. In *Advances in Coastal and Ocean Engineering*; Liu, P.L.F., Ed.; World Scientific Publishing Company: Singapore, 1996; pp. 151–197.
 43. Wang, Z.B.; Hoekstra, P.; Burchard, H.; Ridderinkhof, H.; De Swart, H.E.; Stive, M.J.F. Morphodynamics of the Wadden Sea and its barrier island system. *Ocean. Coast. Manag.* **2012**, *68*, 39–57. [[CrossRef](#)]
 44. Wang, Z.B.; Louters, T.; De Vriend, H.J. Morphodynamic modelling for a tidal inlet in the Wadden Sea. *Mar. Geol.* **1995**, *126*, 289–300. [[CrossRef](#)]
 45. Lesser, G.R.; Roelvink, J.A.; Van Kester, J.A.T.M.; Stelling, G.S. Development and validation of a three-dimensional model. *Coast. Eng.* **2004**, *51*, 883–915. [[CrossRef](#)]
 46. Elias, E.P.L. Morphodynamics of Texel Inlet. Ph.D. Thesis, Delft University of Technology, Delft, The Netherlands, 2006; p. 261. Available online: <https://repository.tudelft.nl/islandora/object/uuid:92ad4ac0-9d54-4f5f-8536-80b7782a6aa6?collection=research> (accessed on 3 July 2019).
 47. Lesser, G.R. An approach to medium-term coastal morphological modelling. Ph.D. Thesis, UNESCO-IHE, Delft, The Netherlands, 2009.
 48. Van der Wegen, M. Modeling Morphodynamic Evolution in Alluvial Estuaries. Ph.D. Thesis, UNESCO-IHE, Delft, The Netherlands, 2009.
 49. Elias, E.P.L.; Hansen, J. Understanding processes controlling sediment transports at the mouth of a highly energetic inlet system (San Francisco Bay, CA). *Mar. Geol.* **2012**, *345*, 207–220. [[CrossRef](#)]
 50. Hibma, A.; De Vriend, H.J.; Stive, M.J.F. Numerical modelling of shoal pattern formation in well-mixed elongated estuaries. *Estuar. Coast. Shelf Sci.* **2003**, *57*, 981–991. [[CrossRef](#)]
 51. Dastgheib, A.; Roelvink, J.A.; Wang, Z.B. Long-term process-based morphological modeling of the Marsdiep tidal basin. *Mar. Geol.* **2008**, *256*, 90–100. [[CrossRef](#)]
 52. Van der Wegen, M.; Roelvink, J.A. Long-term morphodynamic evolution of a tidal embayment using a two-dimensional, process-based model. *J. Geophys. Res.* **2008**, *113*, C03016. [[CrossRef](#)]
 53. Van der Wegen, M.; Wang, Z.B.; Savenije, H.H.G.; Roelvink, J.A. Long-term morphodynamic evolution and energy dissipation in a coastal plain, tidal embayment. *J. Geophys. Res.* **2008**, *113*, F03001. [[CrossRef](#)]
 54. Geleynse, N.; Storms, J.E.A.; Walstra, D.J.R.; Jagers, H.R.A.; Wang, Z.B.; Stive, M.J.F. Controls on river delta formation; insights from numerical modelling. *Earth Planet. Sci. Lett.* **2011**, *302*, 217–226. [[CrossRef](#)]

55. Van Maanen, B.; Coco, G.; Bryan, K.R.; Friedrichs, C.T. Modeling the morphodynamic response of tidal embayments to sea-level rise. *Ocean. Dyn.* **2013**, *63*, 1249. [[CrossRef](#)]
56. Gao, W.; Shao, D.; Wang, Z.B.; Nardin, W.; Yang, W.; Sun, T.; Cui, B. Combined effects of unsteady river discharges and wave conditions on river mouth bar morphodynamics. *Geophys. Res. Lett.* **2018**, *45*, 903–911. [[CrossRef](#)]
57. Gao, W.; Shao, D.; Wang, Z.B.; Nardin, W.; Rajput, P.; Yang, W.; Sun, T.; Cui, B. Long-term cumulative effects of intra-annual variability of unsteady river discharge on the progradation of delta lobes: A modeling perspective. *J. Geophys. Res. Earth Surf.* **2019**, *124*, 960–973. [[CrossRef](#)]
58. Tao, J.; Wang, Z.B.; Zhou, Z.; Xu, F.; Zhang, C.; Stive, M.J.F. A morphodynamic modeling study on the formation of the large-scale radial sand ridges in the Southern Yellow Sea. *J. Geophys. Res. Earth Surf.* **2019**, *124*, 1742–1761. [[CrossRef](#)]
59. Van der Wegen, M. Numerical modeling of the impact of sea level rise on tidal basin morphodynamics. *J. Geophys. Res. Earth Surf.* **2013**, *118*, 447–460. [[CrossRef](#)]
60. Elias, E.P.L.; Teske, R.; Van der Spek, A.; Lazar, M. Modeling tidal inlet morphodynamics on medium timescales. In *The Proceedings of the Coastal Sediments 2015*; Wang, P., Rosati, J.D., Cheng, J., Eds.; CD-ROM: San Diego, CA, USA, 2015; p. 14.
61. Wang, Y.; Yu, Q.; Jiao, J.; Tonnon, P.K.; Wang, Z.B.; Gao, S. Coupling bedform roughness and sediment grain-size sorting in modelling of tidal inlet incision. *Mar. Geol.* **2016**, *381*, 128–141. [[CrossRef](#)]
62. Dissanayake, D.M.P.K.; Ranasinghe, R.; Roelvink, J.A. The morphological response of large tidal inlet / basin systems to relative sea level rise. *Clim. Chang.* **2012**, *113*, 253–276. [[CrossRef](#)]
63. Wang, Z.; Van der Spek, A. Importance of mud for morphological response of tidal basins to sea level rise. In *The Proceedings of the Coastal Sediments 2015*; Wang, P., Rosati, J.D., Cheng, J., Eds.; CD-ROM: San Diego, CA, USA, 2015; p. 10.
64. Hofstede, J.L.A.; Becherer, J.; Burchard, H. Are Wadden Sea tidal systems with a higher tidal range more resilient against sea level rise? *J. Coast. Conserv.* **2018**, *22*, 71–78. [[CrossRef](#)]
65. Becherer, J.; Hofstede, J.; Gräwe, U.; Purkiani, K.; Schulz, E.; Burchard, H. The Wadden Sea in transition—consequences of sea level rise. *Ocean Dyn.* **2018**, *68*, 131–151. [[CrossRef](#)]
66. De Swart, H.E.; Zimmerman, J.T.F. Morphodynamics of tidal inlet systems. *Ann. Rev. Fluid Mech.* **2009**, *41*, 203–229. [[CrossRef](#)]
67. Stive, M.J.F.; Capobianco, M.; Wang, Z.B.; Ruol, P.; Buijsman, M.C. Morphodynamics of a tidal lagoon and adjacent coast. In *Physics of Estuaries and Coastal Seas, Proceedings of the 8th International Biennial Conference on Physics of Estuaries and Coastal Seas, the Hague, Netherlands, 9–12 September 1996*; Dronkers, J., Scheffers, M.B.a.M., Eds.; CRC Press/ Balkema: Boca Raton, FL, USA, 1998; pp. 397–407.
68. Stive, M.J.F.; Wang, Z.B. Morphodynamic modelling of tidal basins and coastal inlets. In *Advances in Coastal Modelling*; Lakkhan, C., Ed.; Elsevier Sciences: Amsterdam, The Netherlands, 2003; pp. 36–392.
69. Townend, I.H.; Wang, Z.B.; Stive, M.J.F.; Zhou, Z. Development and extension of an aggregated scale model: Part 1 Background to ASMITA. *China Ocean. Eng.* **2016**, *30*, 483–504. [[CrossRef](#)]
70. Townend, I.H.; Wang, Z.B.; Stive, M.J.F.; Zhou, Z. Development and extension of an aggregated scale model: Part 2 Extensions to ASMITA. *China Ocean. Eng.* **2016**, *30*, 651–670. [[CrossRef](#)]
71. Van Goor, M.A.; Zitman, T.J.; Wang, Z.B.; Stive MJ, F. Impact of sea-level rise on the morphological equilibrium state of tidal inlets. *Mar. Geol.* **2003**, *202*, 211–227. [[CrossRef](#)]
72. Wang, Z.B.; De Vriend, H.J.; Stive MJ, F.; Townend, I.H. On the parameter setting of semi-empirical long-term morphological models for estuaries and tidal lagoons. In *River, Coastal and Estuarine Morphodynamics*; Dohmen-Janssen, C.M., Hulscher SJ, M.H., Eds.; Taylor & Francis: Didcot, UK; London, UK; Abingdon, UK, 2008; pp. 103–111.
73. Kragtwijk, N.G.; Stive MJ, F.; Wang, Z.B.; Zitman, T.J. Morphological response of tidal basins to human interventions. *Coast. Eng.* **2004**, *51*, 207–221. [[CrossRef](#)]
74. Townend, I.H.; Wang, Z.B.; Rees, J.G. Millennial to annual volume changes in the Humber estuary. *Proc. R. Soc. A* **2007**, *463*, 837–854. [[CrossRef](#)]
75. Wang, Z.B.; Townend, I.H. Influence of the nodal tide on the morphological response of estuaries. *Mar. Geol.* **2012**, *291*, 73–82. [[CrossRef](#)]
76. de Vet, P.L.M.; van Prooijen, B.C.; Colosimo, I.; Steiner, N.; Ysebaert, T.; Herman, P.M.J.; Wang, Z.B. The Inhomogeneous Impact of Storm Events on Intertidal flat Eco-Morphodynamics. *Sci. Rep.* **2019**. Submitted.

77. Van der Wegen, M.; Jaffe, B.; Foxgrover, A.; Roelvink, D. Mudflat morphodynamics and the impact of sea level rise in South San Francisco Bay. *Estuaries Coasts* **2016**, *40*, 37–49. [[CrossRef](#)]
78. Elmilady, H.; van der Wegen, M.; Roelvink, D.; Jaffe, B.E. Intertidal area disappears under sea level rise: 250 years of morphodynamic modeling in San Pablo Bay, California. *J. Geophys. Res. Earth Surf.* **2019**, *124*, 38–59. [[CrossRef](#)]



© 2019 by the authors. Licensee MDPI, Basel, Switzerland. This article is an open access article distributed under the terms and conditions of the Creative Commons Attribution (CC BY) license (<http://creativecommons.org/licenses/by/4.0/>).